ISSN (Print) 1226-1750
ISSN (Online) 2233-6656
Journal of Magnetics 30(4), 519-525 (2025) https://doi.org/10.4283/JMAG.2025.30.4.519

Improvement of Microstructure and Magnetic Properties of Ce-Fe-B Hot-deformed Magnets by $Nd_{70}Cu_{30}$ Doping

Ha-Rim Choi[1], Su-Min Kim[2], Jung-Goo Lee[2], Bo-kyeong Han[3], Haein Choi-Yim[4]*, and Hee-Ryoung Cha[2]*

[1]Nagoya University, Department of Materials Process Enginering, Nagoya, 464-8601, Japan
[2]Korea Institute of Materials Science, Department of Magnetic Materials, Changwon 51508, Republic of Korea
[3]Hyundai, Driving System & Magnetic Material Developmennt Team, Hwaseong-si 18270, Republic of Korea
[4]Sookmyung Women's University, Department of Applied Physics, Seoul 04319, Republic of Korea

(Received 10 July 2025, Received in final form 10 December 2025, Accepted 11 December 2025)

Ce-Fe-B magnets with a medium performance between that of Nd-Fe-B magnets and ferrite magnets were prepared using a hot deformation process. To improve the grain orientation and magnetic properties of Ce-Fe-B hot-deformed magnets, a doping process with an Nd-Cu eutectic alloy was employed. As a result, the coercivity was enhanced from 0.37 to 1.86 kOe by 10 wt.% Nd-Cu doping due to the formation of a distinct grain boundary phases. Despite doping with nonmagnetic Nd-Cu, the remanence increased significantly from 4.45 to 9.31 kG by 10 wt.% Nd-Cu doping because of the improved grain alignment and increasing the saturation magnetization caused by changes in the composition of matrix phases. Microstructural observations revealed that the formation of $Ce(Fe,Co)_2$ granules several tens to hundreds of nanometers in size inside the ribbon flakes was suppressed by Nd-Cu doping, and instead, rare-earth (RE)-rich phases were formed at the grain boundaries and ribbon flake interfaces.

Keywords : Ce-Fe-B magnets, hot deformation, gap magnets

1. Introduction

Ferrites and rare-earth (RE) permanent magnets are two main types of permanent magnets widely used across industry. The ferrite magnets have a low price but their maximum energy product is relatively low, less than 4.8 MGOe, which limits their applications in various fields [1]. Nd-Fe-B-based magnets have attracted considerable attention for decades owing to their excellent magnetic properties of over 25 MGOe, and their demand has recently increased in electric/hybrid vehicles, industrial motors, and wind turbines [2-6]. However, the increasing demand for Nd-Fe-B-based magnets could lead to rising Nd prices and an imbalanced utilization of rare-earth (RE) sources. Therefore, the development of low-cost permanent magnets that contain no or only small amounts of critical RE elements such as Nd and Pr, and have performances between hard ferrite and Nd-Fe-B is becoming increasingly important. Ce, the cheapest and most abundant rare earth element, is one of the candidate elements to replace critical rare earth elements, such as Nd and Pr, in RE-Fe-B-based magnets [7-9], and many efforts have been made to investigate the effect of substituting Nd with Ce in RE-Fe-B-based magnets [10-14]. However, since the intrinsic magnetic properties of the $Ce_2Fe_{14}B$ compound ($4\pi M$ = 11.7 KG, H_A = 26 kOe, T_c = 424 K) are lower than those of the $Nd_2Fe_{14}B$ compound ($4\pi M$ = 16 KG, H_A = 73 kOe, T_c = 585 K), there is a limit to achieving magnetic properties equivalent to those of Nd-Fe-B magnets by replacing Nd with Ce [15, 16]. However, $Ce_2Fe_{14}B$ compounds have considerable potential as so-called 'Gap Magnet' with low-cost and medium performance between hard ferrites and Nd-Fe-B magnets.

Optimizing the microstructure of magnets is essential to improving their magnetic properties. Grain refinement and grain boundary control are necessary to enhance the magnetic properties of RE-Fe-B magnets. Melt-spinning and hot deformation processes are well-known effective methods for fabricating ultrafine-grained anisotropic magnets [16-19]. The melt-spun powders had ultrafine grains but were crystallographically isotropic. Hence, a

*Co-corresponding author: Tel: +82-2-710-9239
e-mail: haein@sookmyung.ac.kr (H. C. Yim)
Tel: +82-55-280-3525, Fax: +82-55-280-3289
E-mail: h.cha@kims.re.kr (H. R. Cha)

hot deformation process should be followed for anisotropic bulk magnets. During hot deformation, the c-axis of the grains is aligned parallel to the pressing direction by grain boundary sliding and grain rotation, resulting in a [001] texture [20, 21].

For Ce-Fe-B hot-deformed magnets, however, the [001] texture is not well developed due to the formation of the $CeFe_2$ phase with a high melting point of 1198 K and a lack of low-melting-point Ce-rich grain boundary phases [22]. Nevertheless, because Ce-Fe-B magnets have the potential to be cost-effective permanent magnets with better magnetic properties than hard ferrites, suppressing the formation of $CeFe_2$ and improving the c-axis orientation of Ce-Fe-B hot-deformed magnets are of great interest for high-performance Ce-Fe-B magnets. The addition of low-melting-point alloys to form continuous grain-boundary phases could be a good approach for fabricating high-performance hot-deformed Ce-Fe-B magnets. However, most studies have focused on improving the coercivity of Ce-Fe-B hot-deformed magnets by adding low-melting-point alloys, and there is a relative lack of systematic discussion on the correlation with grain orientation.

Therefore, in this study, to develop a [001] texture for Ce-Fe-B hot-deformed magnets, a eutecitic Nd-Cu alloy was doped into Ce-Fe-B hot-deformed magnets. A detailed understanding of the relationship between the microstructure and magnetic properties of Ce-Fe-B hot-deformed magnets doped with Nd-Cu was investigated.

2. Experimental

Initially, melt-spun ribbons with nominal compositions of $Ce_{13.6}Fe_{73.6}B_{5.6}Co_{6.6}Ga_{0.6}$ (at.%) were prepared by an arc-melting and melt-spinning process with a wheel speed of 20 m/s under an argon atmosphere. The melt-spun ribbons were pulverized into powders with a size of 125-300 μm in a glove box with oxygen content below 0.1 ppm. For the grain boundary modification, $Nd_{70}Cu_{30}$ (at.%) eutectic alloys with a melting point of approximately 793 K were used as doping materials. The $Nd_{70}Cu_{30}$ (at.%) ribbons were also prepared by an arc-melting and melt-spinning process with a wheel speed of 30 m/s and were then ground into 53-125 μm particles. Before the hot deformation process, the $Ce_{13.6}Fe_{73.6}B_{5.6}Co_{6.6}Ga_{0.6}$ powders were mixed with 0 wt.%, 5 wt.%, 10 wt.%, and 15 wt.% of $Nd_{70}Cu_{30}$ powders. The mixture powders were then hot-pressed at 973 K under 200 MPa in a vacuum to obtain high-density isotropic compacts, followed by hot deformation at 973 K until a 75% height reduction was achieved. The optimized parameters for these processes were adopted from previous studies [23].

To determine the crystallographic structure and the alignment of the grains in the magnets, X-ray diffraction (XRD, Rigaku, D/Max-2500VL/PC) measurements were performed using Cu-Kα radiation. The magnetic properties of the magnets were measured using a vibrating sample magnetometer (VSM, Microsense, EZ9) after pre-magnetization with a 5 T pulsed magnetic field. The microstructures and elemental distributions of the initial powders and hot-deformed magnets were examined using field-emission scanning electron microscopy (FE-SEM; JEOL, JSM-7001F) and scanning transmission electron microscopy (STEM; Thermo Fisher Scientific, Talos F200X), combined with energy-dispersive X-ray spectroscopy (EDS).

3. Results and Discussion

Fig. 1(a) shows XRD patterns of Ce-Fe-B melt-spun ribbons. The tetragonal matrix phase (space group $P4_2/$

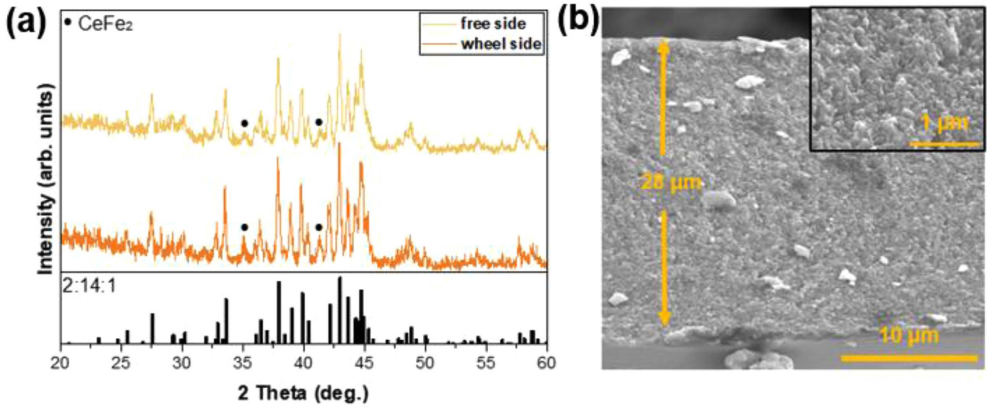

Fig. 1. (Color online) (a) XRD patterns and (b) cross-sectional SEM images of initial melt-spun powders.

mnm) was mainly observed on both the wheel and the free side of the ribbons, and $CeFe_2$ peaks were also observed at 34.7 and 40.9 degrees. The ribbon thickness and grain size were determined from the fracture surface images of the initial ribbons (Fig. 1(b)). The inset shows a magnified image of the grains within the ribbon. The thickness and average grain size of the ribbons were approximately 28 μm and 40 nm, respectively. The grain size was uniform on both the wheel and free surfaces, and no abnormal grain growth regions were observed.

The ribbon powders were fabricated into anisotropic bulk magnets using hot-pressing and hot deformation processes. Fig. 2 shows the hysteresis loops of un-doped and 10 wt.% Nd-Cu doped hot-deformed magnets, and the coercivity, remanence, and $(BH)_{max}$ of the hot-deformed magnets as a function of the Nd-Cu doping content. The coercivity of the hot-deformed magnets increased gradually as the doping amount increased, whereas the remanence and $(BH)_{max}$ increased as the Nd-Cu doping amount increased to 10 wt.%, and then decreased again for the 15 wt.% Nd-Cu doped magnets. The coercivity of magnets can be increased by modifying the grain boundary thickness and composition. A thick and continuous nonmagnetic grain boundary can enhance the coercivity of magnets by inducing magnetic decoupling between neighboring grains. In general, the volume fraction of the magnetic phase, saturation magnetization, and degree of grain alignment contribute to the remanence of magnets. Adding nonmagnetic Nd-Cu alloys should decrease the remanence of magnets due to the increased nonmagnetic volume fraction. However, the remanence tends to increase as Nd-Cu doping amount increases. To investigate the effect of Nd-Cu doping on

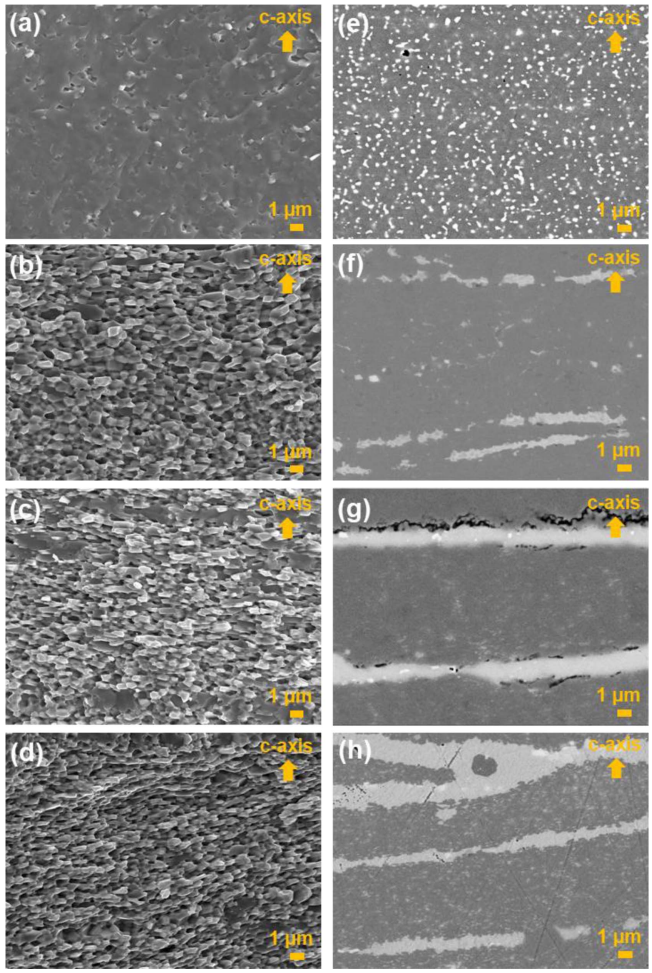

Fig. 3. (Color online) (a, b, c, d) Fracture surface secondary electron (SE) images and (e, f, g, h) back-scattered electron (BSE) images of (a, e) un-doped, (b, f) 5 wt.% doped, (c, g) 10 wt.% doped and (d, h) 15 wt.% doped hot-deformed magnets.

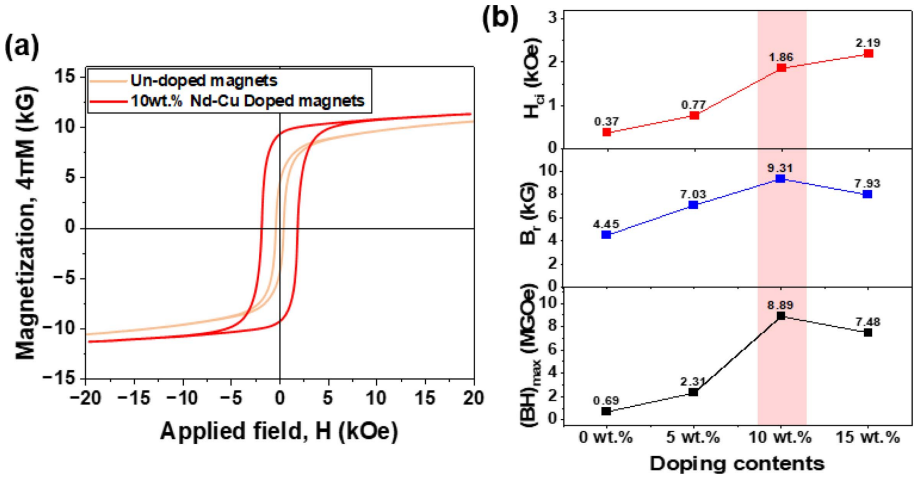

Fig. 2. (Color online) (a) Hysteresis loops of un-doped and 10 wt.% doped hot-deformed magnets and (b) H_{cj}, B_r, and $(BH)_{max}$ of hot-deformed magnets as a function of Nd-Cu doping content.

magnetic properties, microstructural observations were performed. Fracture surface and backscattered electron (BSE) images of the un-doped and 5, 10, 15 wt.% Nd-Cu doped hot-deformed magnets are shown in Fig. 3. In the cross-sectional fracture images of the un-doped and 5 wt.% Nd-Cu doped hot-deformed magnets, most of the grains are not well distinguished, whereas the grains of the 10 and 15 wt.% Nd-Cu doped magnets are clearly distinguished. In general, RE-Fe-B permanent magnets exhibit completely brittle fracture characteristics at the grain boundaries, and the much lower hardness of the RE-rich phase along the grain boundary compared to that of the matrix phase is the main reason for intergranular fracture [24]. However, the absence of a RE-rich phase could induce transgranular fracture, which could decrease the coercivity of the magnets owing to magnetic coupling between neighboring grains. The un-doped hot-deformed magnet had spherical grains and faint grain boundaries, while the 5, 10, 15 wt.% Nd-Cu doped magnet has platelet-shaped grains that are elongated along the crystallographic a-axis and well-aligned in one direction, which is a typical microstructure of anisotropic hot-deformed magnets. As shown in Fig. 3(e), the BSE image of the un-doped Ce-Fe-B magnet is mainly composed of the $Ce_2Fe_{14}B$ phase, corresponding to the dark gray contrast, and a large number of secondary phases with bright contrast. However, bright areas were rarely observed in the Nd-Cu doped hot-deformed magnets (Fig. 3(d)).

STEM analysis was performed to identify the secondary phase observed in the un-doped hot-deformed magnets (Fig. 3(b)). Fig. 4(a) shows the high-angle annular dark-field scanning transmission electron microscopy (HAADF-STEM) images and EDS elemental maps of the un-doped hot-deformed magnets. The EDS elemental map confirmed that the secondary phase existed as precipitates several tens to hundreds of nanometers in size. Fig. 4(b) and (c) show the EDS line scan profiles across the secondary phase, indicated by the yellow arrow, and the selected area electron diffraction (SAED) pattern, indicated by the red circle in Fig. 4(a), respectively. The secondary phase shown in Fig. 4(a) contains Ce, Fe, and Co (Fig. 4(b)), and these phases were indexed as a $Ce(Fe,Co)_2$ phase having a cubic Laves phase structure with space group $Fd\bar{3}m$, as illustrated in Fig. 4(c). Although $Nd_2Fe_{14}B$ and $Ce_2Fe_{14}B$ compound have the same crystalstructure, their magnetism and phase diagram are quite different due to the different valence states and existence of $CeFe_2$ phase. It has been reported that the $CeFe_2$ phase is inevitably formed in Ce-Fe-B ternary system [25]. The $CeFe_2$ phase exhibits paramagnetism at room temperature because of its low Curie temperature (235 K), which monotonically decreases with increasing Co concentration [26]. Furthermore, the melting point of the $CeFe_2$ phase is approximately 1198 K, which is higher than the hot deformation processing temperature. Thus, it can exist as precipitates at the grain boundaries and interfere with grain alignment during the hot deformation process. However, regarding the substitution of Ce by Nd in the Ce-Fe-B magnets, the substitution energy in the $CeFe_2$ phase is positive, whereas in the $Ce_2Fe_{14}B$ phase it is negative. This

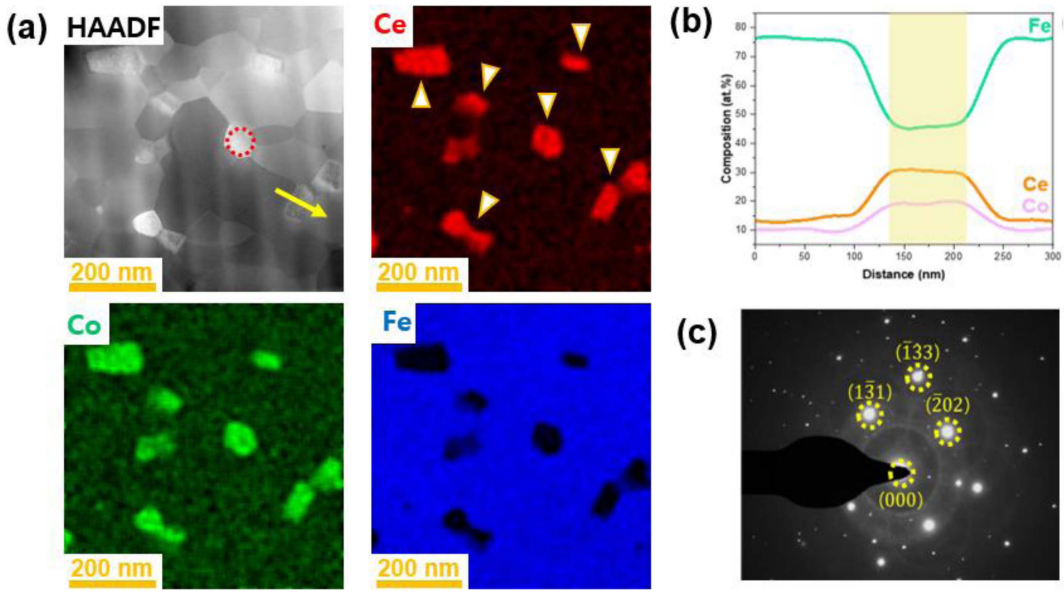

Fig. 4. (Color online) (a) HAADF-STEM image and EDS elemental mappings of un-doped hot-deformed magnet; (b) EDS line scan profiles across the secondary phase marked by yellow arrow; and (c) SAED pattern of the area marked by red dashed circle.

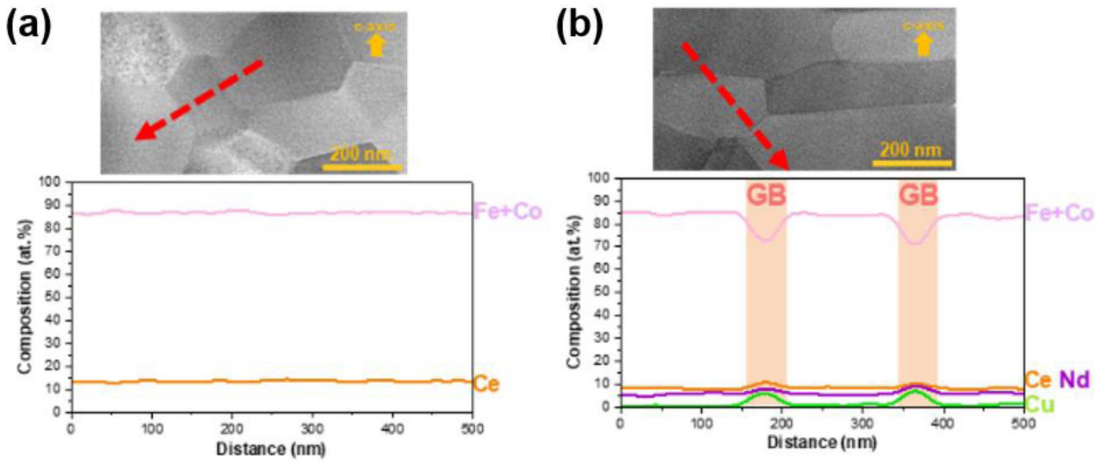

Fig. 5. (Color online) HAADF-STEM image and EDS line scan profiles across the grain boundary phases of (a) un-doped and (b) 10 wt.% doped hot-deformed magnets.

indicate that partial substitution of Ce by Nd reduces the phase stability and driving force for phase formation of $CeFe_2$ [27]. It implies that compositional change of the magnets by addition of Nd-based alloy can suppress or reduce the formation of $CeFe_2$, which is consistent with the results in Fig. 3.

Figure 5 shows HAADF-STEM micrographs and line concentration profiles across the grain boundary phases of the un-doped and 10 wt.% Nd-Cu doped hot-deformed magnets. The 10 wt.% Nd-Cu doped hot-deformed magnets show a relatively high concentration of RE elements at the grain boundaries (Fig. 5(b)). However, the un-doped hot-deformed magnets did not exhibit clear grain boundaries and no segregation of RE elements (Fig. 5(a)). The presence of RE-rich grain boundary phases with melting points below the processing temperature can significantly assist in the formation of platelet-shaped grains within the magnets and improve the alignment of the grain c-axis via grain boundary sliding during the hot deformation process. The chemical composition of RE-rich grain boundaries of the 10 wt.% doped hot-deformed magnets were close to ~$Nd_{8.4}Ce_{11.0}Fe_{66.5}Co_{7.8}Cu_{6.4}$ at.%. The formation of uniform and continuous nonmagnetic grain boundaries contributes to exchange decoupling between neighboring grains, thereby enhancing the coercivity. However, a large amount of ferromagnetic element was detected at the RE-rich grain boundaries, which causes a decrease in coercivity. Therefore, it is necessary to further reduce the Fe and Co concentrations at the grain boundaries to achieve high coercivity. On the other hand, Fig. 5(b) shows that approximately 5 at.% Nd was contained within the grains, indicating that Nd diffused into the grains by substituting for Ce in the matrix phase during the hot deformation process. The chemical composition of matrix phase also was calculated to be $(Nd_{0.42}Ce_{0.58})_2(Fe_{91}Co_{0.9})_{14}B_1$ at.% from Fig. 5(b). As the Nd content in the matrix phase increases, the saturation magnetization of the magnet could increase; thus, the remanence of the magnet can also improve as the substitution amount increases. However, it is difficult to accurately determine the substitution ratio of Ce to Nd in the matrix because the substitution ratio of Ce to Nd in the grains inside the magnet varies depending on the position. Regarding the overall composition of the magnet, the Ce:Nd weight ratio in the whole magnet is calculated to be 75.8:24.2 for 10 wt.% Nd-Cu doped magnets. Assuming that Nd and Ce are evenly distributed throughout and the saturation magnetization changes linearly according to the composition ratio, the saturation magnetization could increase by approximately 8.88% for 10 wt.% Nd-Cu doped magnets. This mostly compensates for the decrease in saturation magnetization caused by the increase in the nonmagnetic volume fraction due to the Nd-Cu doping.

An XRD analysis was performed to quantify the degree of alignment of the internal grains. Fig. 6 shows the XRD patterns of the magnets with different Nd-Cu doping amounts. The degree of alignment (DoA) was defined as the intensity ratio of the I(105)/I(006) peaks [28, 29]. The DoA of the un-doped hot-deformed magnet was approximately 0.318. However, it increased with Nd-Cu doping, and the highest DoA was shown in the 10 wt.% Nd-Cu doped hot-deformed magnet as 1.014. The enhancement of DoA was attributed to the relatively distinct RE-rich grain boundaries formed by the doping of the Nd-Cu eutectic powders. The melted grain boundaries

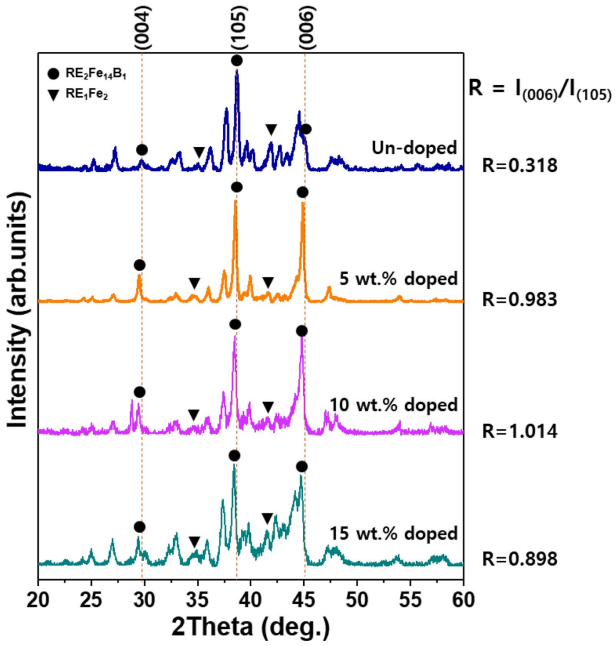

Fig. 6. (Color online) XRD patterns of the un-doped hot-deformed magnets and doped hot-deformed magnets with different Nd-Cu doping.

facilitate grain rotation and sliding, making it easier during hot deformation. The improved grains orientation is one of the main reasons for the enhanced remanence of the magnets from 4.45 to 9.31 kG in Fig. 2. However, the 15 wt.% Nd-Cu doped magnet shows a decreased DoA compared to that of the 10 wt.% Nd-Cu doped magnets. During the hot deformation process, the stress was significantly reduced from 229 MPa for the 10 wt.% doped magnets to 183 MPa for the 15 wt.% doped magnets, even though the hot deformation was performed under the same conditions. Therefore, this is explained by the excessive addition of Nd-Cu eutectic powders, which could disturb the alignment of the grains because the liquid Nd-Cu alloys could relieve the compressive stress and reduce the grain rotation torque. In addition, with regard to stress, Wang *et al.* also reported that the melted RE-rich phase aggregated at the flake interface can promote grain growth by relieving the stress field applied to the neighboring grains and consequently disturb grain orientation during hot deformation [30].

4. Conclusion

The effect of Nd-Cu doping on the grain alignment and magnetic properties of Ce-Fe-B hot-deformed magnets was investigated. With the doping of the Nd-Cu eutectic alloy, the $CeFe_2$ phase inside the flakes, which disturbed the grain alignment during the hot deformation process, was removed. The coercivity and remanence of the magnets were significantly enhanced after the Nd-Cu doping. With the doping of Nd-Cu alloys, a relatively distinct RE-rich phase was formed, which helped the grains align during the hot deformation process. The 10 wt.% doped hot-deformed magnets achieved a maximum energy product of about 9 MGOe, which exceeds the maximum energy product of conventional ferrite magnets. The coercivity can be further improved by modifying grain boundaries phase through applying additional grain boundary diffusion processes, and developed magnets can be applied to speakers, microphone, automobile electric motors, etc. that use ferrite magnets.

Acknowledgement

This research was supported by the Nano & Material Technology Development Program through the National Research Foundation of Korea (NRF) funded by the Ministry of Science and ICT (RS-2023-00282305), and a Korea Evaluation Institute of Industrial Technology (KEIT) grant funded by the Korean Government (MOTIE) (No. 00431940).

References

[1] W. Zuo, S. Zuo, R. Li, T. Zhao, F. Hu, J. Sun, X. Zhang, J. Liu, and B. Shen, J. Alloys Compd. **695**, 1786 (2017).
[2] K. Hioki, Sci. Technol. Adv. Mater. **22**, 72 (2021).
[3] H. Sepehri-Amin, T. Ohkubo, T. Shima, and K. Hono, Acta Mater **60**, 819 (2012).
[4] Y. H. Hou, Y. L. Wang, Y. L. Huang, Y. Wang, S. Li, S. C. Ma, Z. W. Liu, D. C. Zeng, L. Z. Zhao, and Z. C. Zhong, Acta Mater. **115**, 385 (2016).
[5] J. D. Widmer, R. Martin, and M. Kimiabeigi, Sustain. Mater. Technol. **3**, 7 (2015).
[6] O. Gutfleisch, M. A. Willard, E. Brück, C. H. Chen, S. G. Sankar, and J. P. Liu, Adv. Mater. **23**, 821 (2011).
[7] D. Liu, T. Ma, L. Wang, Y. Liu, T. Zhao, F. Hu, J. Sun, and B. Shen, J. Phys. D **52**, 135002 (2019).
[8] H. Peng, D. Yu, X. Bai, X. Lin, Y. Mao, Z. Wang, and Y. Luo, J. Rare Earths. **39**, 986 (2021).
[9] G. Kim, T. Kim, H. Cha, S. Lee, D. Kim, Y. Kim, and J. Lee, J. Mater. Sci. Technol. **126**, 71 (2022).
[10] M. Xing, J. Han, Z. Lin, F. Wan, C. Li, S. Liu, C. Wang, J. Yang, and Y. Yang, J. Magn. Magn. Mater. **331**, 140 (2013).
[11] C. Zhou, F. E. Pinkerton, and J. F. Herbst, Scr. Mater. **95**, 66 (2015).
[12] C. Yan, S. Guo, R. Chen, and D. Lee, Chin. Phys. B **23**, 107501 (2014).
[13] X. Tang, H. Sepehri-Amin, T. Ohkubo, M. Yano, M. Ito,

A. Kato, N. Sakuma, T. sshoji, T. Schrefl, and K. Hono, Acta Mater. **144**, 884 (2018).
[14] Y. L. Huang, Z. H. Li, X. J. Ge, Z. Q. Shi, T. H. Hou, G. P. Wang, Z. W. Liu, and Z. C. Zhong, J. Alloys Compd. **797**, 1133 (2019).
[15] R. K. Mishra, V. Panchanathan, and J. J. Croat, J. Appl. Phys. **73**, 6470 (1993).
[16] G. Kim, H. Cha, Y. Baek, Y. Kim, D. Kim, Y. Kim, and J. Lee, J. Magn. **25**, 197 (2020).
[17] J. J. Croat, IEEE Trans. Magn. **25**, 3550 (1989).
[18] J. Yoo, H. Cha, D. Kim, Y. Kim, and J. Lee, J. Magn. **25**, 29 (2020).
[19] D. Lee, J. S. Hilton, C. H. Chen, M. Q. Huang, Y. Zhang, G. C. Hadjipanayis, and S. Liu, IEEE Trans. Magn. **40**, 2904 (2004).
[20] H. Y. Yasuda, M. Kumano, T. Nagase, R. Kato, and H. Shimizu, Scr. Mater. **65**, 743 (2011).
[21] W. Grünberger, D. Hinz, A. Kirchner, K. Müller, and L. Schultz, J. Alloys Compd. **257**, 293 (1997).
[22] A. V. Morozkin, Y. D. Seropegin, A. V. Gribanov, and J. M. Barakatova, J. Alloys Compd. **256**, 175 (1997).
[23] H. Cha, S. Liu, J. Yu, H. Kwon, Y. Kim, and J. Lee, IEEE Trans. Magn. **51**, 2101704 (2015).
[24] W. Liu and J. Wu, J. Alloys Compd. **458**, 292 (2018).
[25] Q. Jiang, W. Lei, L. He, Q. Zeng, S. U. Rehman, L. Zhang, R. Liu, S. Ma, and Z. Zhong, J. Alloys Compd. **775**, 449 (2019).
[26] H. Fukuda, H. Fujii, H. Kamura, Y. Hasegawa, T. Ekino, N. Kikugawa, T. Suzuki, and T. Fujita, Phys. Rev. B **63**, 054405 (2001).
[27] X. Liu, I. Nlebedim, and Z. Altounian, IEEE Trans. Magn. **57**, 2101204 (2021).
[28] Q. Yang, R. Wang, Y. Liu, J. Li, H. Chen, and X. Yang, J. Magn. Magn. Mater. **511**, 166940 (2020).
[29] Z. Guo, M. Li, J. Wang, Z. Jing, M. Yue, M. Zhu, and W. Li, AIP Adv. **8**, 056234 (2018).
[30] Z. Wang, K. Pei, J. Zhang, R. Chen, W. Xia, J. Wang, M. Li, and A. Yan, Acta Mater. **167**, 103 (2019).